Journal of Structural Geology, Vol. 10, No. 6, pp. 607 to 623, 1988
Printed in Great Britain

0191-8141/88 $03.00 + 0.00

Description and classification of folds in single surfaces

ROBERT J. TWISS

Geology Department, University of California at Davis, Davis, CA 95616, U.S.A.

(*Received* 9 *October* 1987; *accepted in revised form* 1 *May* 1988)

Abstract—I propose a new three-parameter description of fold style in folded surfaces based on the ratio of the amplitude to the half-wavelength (the aspect ratio P), the maximum angle of relative rotation of opposite limbs of the fold (the folding angle ϕ), and a measure of the relative curvature at the fold closure (the bluntness b). For symmetric folds, the first two parameters define a trapezoid that circumscribes the fold and provides the primary criterion for the classification of fold style. Within a given trapezoid, fold style variations are defined by the bluntness. Perfect folds in profile are defined to have a single hinge with perfectly straight limbs tangent to hinge zones that are perfect circular arcs. An analytic description of the variation in perfect fold geometry defines the limits for all natural single-hinged folds.

The proposed system includes folds with folding angles both less than and greater than isoclinal folds, it applies to both single-hinged and multiple-hinged folds, and it also can be extended to apply to asymmetric folds. Previously proposed two-parameter classification systems can only describe folds that are restricted to a specific surface through the three-parameter fold style space proposed here.

INTRODUCTION

A FOLD style is the combination of the geometric and morphologic characteristics that distinguish one type of fold from all others. An element of fold style is a quantitative measure or a qualitative description of such a distinctive characteristic, and a set of fold style elements serves objectively to characterize the unique qualities of the many different types of folds that are observed in deformed rocks. The elements of fold style can be separated into those that describe folds in a single surface, in a single layer, and in a multilayer.

Ultimately we would like to correlate the style of folding with the mechanism of formation and the strain distribution, although the correspondence need not be one-to-one. To that end, it is necessary to have a system of description and classification of folds that is practical and that highlights the significant differences among fold styles. Numerous authors have proposed such systems, among which are classifications for multilayer folds (Turner & Weiss 1963, Hansen 1971), for single layer folds (Ramsay 1967) and for folds in single surfaces (Fleuty 1964, Ramsay 1967, Stabler 1968, Hudleston 1973). Hudleston (1973) presents a brief overview of a variety of classification schemes with extensive references to work in the field.

In this paper I propose a new three-parameter classification of folds in single surfaces that permits a more precise description of fold geometry and encompasses a broader range of geometries than the two-parameter classifications proposed by Ramsay (1967), Stabler (1968) and Hudleston (1973). The scheme also lends itself to a relatively simple 'visual' classification of folds.

In the following discussion, I use the term *hinge* in its usual definition as the point or points of maximum curvature between two adjacent inflection points on the profile of a folded surface. I use the term *closure* to refer both to the point of maximum curvature of single-hinged folds (Fig. 1a), and to the point of minimum curvature between hinges of double-hinged folds (Fig. 1b). For hinge zones and closure zones characterized by circular arcs, the hinge and closure points are defined to be at the midpoint of the arc.

I define *perfect folds* to be single-hinged folds which in profile have limbs that are perfectly straight and hinge zones that are perfect circular arcs (Fig. 2). The limbs join the hinge zone at the point where the straight limbs are tangent to the circular hinge zone (Fig. 2a). Perfect folds may vary in geometry between the two extremes of (i) perfect chevron folds, for which the two limbs are straight and there is no hinge zone (Fig. 2b), and (ii) perfect circular folds, for which the hinge zone is a single arc of a circle and there are, strictly speaking, no limbs (Fig. 2c). All other folds, which includes essentially all natural folds, are referred to as *imperfect folds*. The geometry of perfect folds is a convenient reference against which to compare imperfect fold geometries.

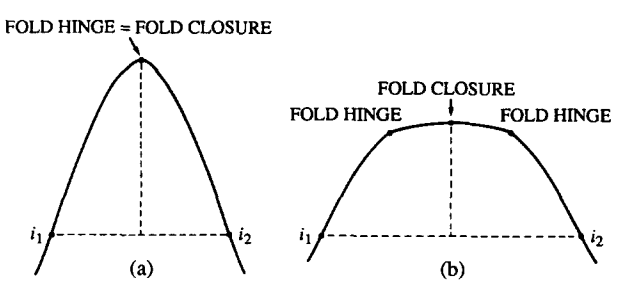

Fig. 1. The closure of a fold in profile. (a) On a single-hinged fold, the closure and the hinge are identical and mark the point of maximum curvature, or the midpoint on the arc of maximum curvature. (b) On a double-hinged fold, the closure is the point of minimum curvature, or the midpoint on the arc of minimum curvature, between the hinges of the fold.

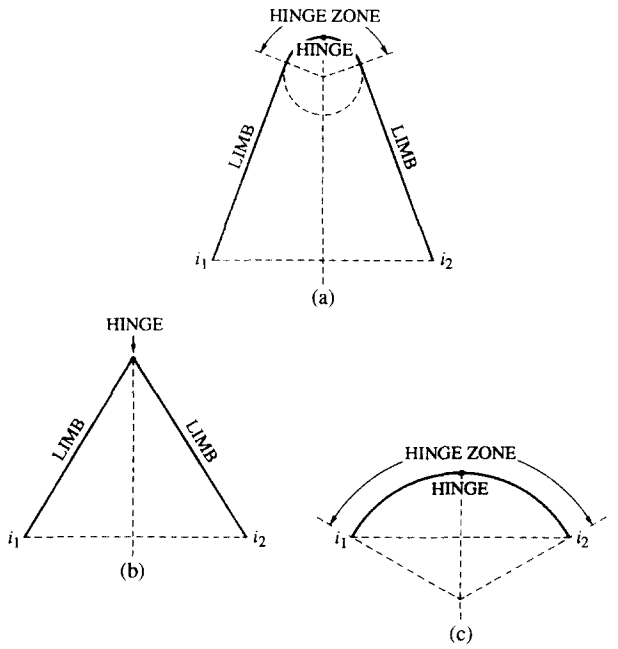

Fig. 2. The geometry of perfect folds. (a) A perfect fold has a single hinge and in profile has perfectly straight limbs which are tangent to hinge zones that are perfectly circular arcs. (b) A perfect chevron fold has no hinge zone. (c) A perfect circular fold has no limbs.

ELEMENTS OF FOLD STYLE FOR SYMMETRIC FOLDS

Symmetric folds are characterized in profile by a mirror plane of symmetry that passes through the closure and is normal to, and bisects, the median line segment M between adjacent inflection points i_1 and i_2 (Ramsay 1967, pp. 351 and 357). The geometry of any such fold may be described with reference to a *circumscribed trapezoid* (Fig. 3) whose base is the median line segment M, whose sides are tangent to the fold limbs at the inflection points and whose top is parallel to the base and tangent to the fold at the closure. The three elements of fold style that characterize the geometry of a half-wavelength fold in a single surface are related to this trapezoid and include the aspect ratio P, the folding angle ϕ, and the bluntness b. I discuss these in order below.

Aspect ratio P

Most authors recognize the amplitude A and the wavelength λ as significant characteristics in describing a fold. Both quantities, however, describe an aspect of the scale of the fold as well as of the geometry. Similarities in the geometry of different folds, independent of scale, are revealed by the ratio of the amplitude to the half wavelength (cf. Hansen 1971), which I refer to as the *aspect ratio P*.

In terms of the circumscribed trapezoid, the amplitude A is the perpendicular distance from the base to the top of the trapezoid, and the half wavelength $\lambda/2$ is the length M of the trapezoid base, which is the distance between

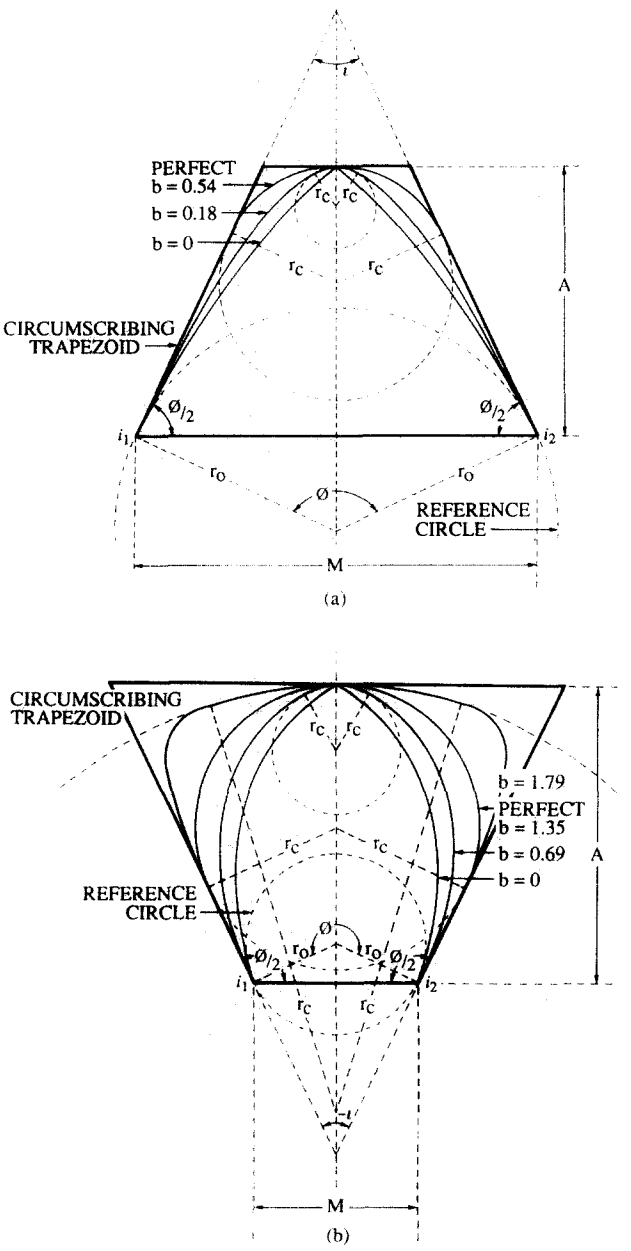

Fig. 3. The circumscribed trapezoid defines the aspect ratio $P = A/M$, the folding angle ϕ and interlimb angle ι of symmetric folds. The bluntness b distinguishes folds of different style within a given trapezoid. r_c labels the radii of closure curvature; r_0 is the radius of curvature for the reference circle. (a) For an acute fold, the half-folding angle $\phi/2$ is an acute angle. For the circumscribing trapezoid shown here, $P = 0.67$, $\phi = 130°$. For the three folds shown within the one trapezoid, $b = 0.54$, 0.18 and 0. The first fold is a perfect fold. (b) For an obtuse fold, the half-folding angle $\phi/2$ is an obtuse angle. For this circumscribing trapezoid, $P = 1.8$, $\phi = 230°$. For the four folds shown within the trapezoid, $b = 1.79$, 1.35, 0.69 and 0. The value of 1.35 is for the perfect fold.

adjacent inflection points of the fold (Fig. 3). Thus

$$P = \frac{A}{M}. \tag{1}$$

The aspect ratio for most folds falls within the range $0.1 \leq P \leq 10$. The change in geometry between 0.1 and 1, however, is comparable to the change between 1 and 10. Thus I use a logarithmic scale for plotting the aspect ratio and for defining the five categories of wide, broad, equant, short and tall folds (Table 1).

Table 1. Aspect ratio

Descriptive term	Aspect ratio (P) $P = A/M$	Log (P)
Wide	$0.1 \leq P < 0.25$	$-1 \leq \log P < -0.6$
Broad	$0.25 \leq P < 0.63$	$-0.6 \leq \log P < -0.2$
Equant	$0.63 \leq P < 1.58$	$-0.2 \leq \log P < 0.2$
Short	$1.58 \leq P < 4$	$0.2 \leq \log P < 0.6$
Tall	$4 \leq P < 10$	$0.6 \leq \log P < 1$

Table 2. Tightness of folds

Descriptive terms		Folding angle	Interlimb angle
Acute	Gentle	$0 < \phi < 60$	$180 > \iota > 120$
	Open	$60 \leq \phi < 110$	$120 \geq \iota > 70$
	Close	$110 \leq \phi < 150$	$70 \geq \iota > 30$
	Tight	$150 \leq \phi < 180$	$30 \geq \iota > 0$
Isoclinal		$\phi = 180$	$\iota = 0$
Obtuse	Fan	$180 < \phi < 250$	$0 > \iota > -70$
	Involute	$250 \leq \phi \leq 360$	$-70 \geq \iota \geq -180$

Folding angle ϕ

The *folding angle* ϕ is the sum of the two internal base angles of the circumscribed trapezoid (Fig. 3a & b). It is a measure of the maximum amount of rotation that one limb has experienced relative to the other during the folding. ϕ is also the angle between the two normals to the fold limbs contructed at the inflection points (Fig. 3a & b).

I refer to folds having acute base angles ($\phi/2 < 90°$) as *acute folds* and those with obtuse base angles ($\phi/2 > 90°$) as *obtuse folds*. These types are separated by *isoclinal folds*, for which $\phi/2 = 90°$ or $\phi = 180°$. Acute folds can be divided into the standard categories for the tightness of folding proposed by Fleuty (1964) of gentle, open, close and tight (Table 2). I divide obtuse folds into fan folds and involute folds (Table 2).

The interlimb angle ι (Ramsay 1967) is the supplement of the folding angle ($\iota = 180° - \phi$). Thus the folding angle increases as the amount of folding increases, whereas the interlimb angle decreases, and the folding angle increases naturally above 180° to include obtuse folds (Fig. 3b), whereas to describe these folds with the interlimb angle, a specific definition of negative interlimb angles must be made (see Table 2).

The bluntness ratio B *and the bluntness* b

The *bluntness* of a fold is a measure of how rounded or angular the closure is. The *bluntness ratio B* is defined as the ratio of the radius of curvature at the fold closure r_c to the radius of curvature of the reference circle r_0, which is taken as the circle tangent to both fold limbs at the inflection points (Fig. 3)

$$B = \frac{r_c}{r_0}. \tag{2}$$

The *bluntness b* is defined in terms of the bluntness ratio and the radii of curvature of the closure and the reference circles by

$$b = \begin{cases} B & = r_c/r_0 \quad \text{for } r_c \leq r_0 \\ 2 - 1/B & = 2 - r_0/r_c \quad \text{for } r_c \geq r_0 \end{cases}. \tag{3}$$

This definition of the bluntness b eliminates the problem that the bluntness ratio B blows up to infinity for double-hinged folds with very large closure radii. In this extreme of the range, very minor changes in geometry lead to major changes in B, making it of limited usefulness in the practical classification of folds. The bluntness b, however, varies continuously and smoothly from 0 to 2 as the closure radius of curvature increases from 0 to ∞. Thus for very flat closures, only minor changes in fold geometry produce very large changes in B, but only minor changes in b. Although the geometrical analysis must be done using the bluntness ratio B, the results are converted to the bluntness b for all plotting and classification.

As I will show in the following discussion, the value of $b = 1$ is a geometrically critical value, separating acute perfect folds from obtuse perfect folds, and single-hinged from double-hinged folds. The symmetry of b about the value $b = 1$ is therefore a convenient feature for classification. Regardless of folding angle or aspect ratio, all perfect chevron folds are characterized by $b = 0$ (Fig. 2b), all perfect circular folds are characterized by $b = 1$ (Fig. 2c), and all folds with perfectly flat closures are characterized by $b = 2$.

The bluntness ratio B is comparable to the inverse of the sharpness defined for single-hinged folds by Ramsay (1967), except that the definition of the reference circle is different. In Ramsay's definition, the radius of the reference circle is $M/2$, whereas here it is

$$r_0 = \frac{M}{2 \sin \phi/2}. \tag{4}$$

The sharpness blows up to infinity for chevron folds, with the result that very minor changes in the geometry of folds with sharp hinges produce extremely large changes in the sharpness, limiting the usefulness of this measure for classifying folds. Moreover, the sharpness does not always give a consistent measure of fold geometry. For example, for a series of perfect circular folds having the same constant curvature but varying folding angle or aspect ratio, the sharpness varies whereas the bluntness is constant. This difference results from the different definition of the reference radius r_0.

Folds are conveniently subdivided according to their bluntness into sharp, angular, subangular, subrounded, rounded and blunt folds, as defined in Table 3 (see Fig. 9).

Table 3. Bluntness of folds

Descriptive term	Bluntness (b)	Bluntness ratio (B)
Sharp	$0.0 \leq b < 0.1$	$0.0 \leq B < 0.1$
Angular	$0.1 \leq b < 0.2$	$0.1 \leq B < 0.2$
Subangular	$0.2 \leq b < 0.4$	$0.2 \leq B < 0.4$
Subrounded	$0.4 \leq b < 0.8$	$0.4 \leq B < 0.8$
Rounded	$0.8 \leq b \leq 1$	$0.8 \leq B \leq 1$
Blunt	$1 < b \leq 2$	$1 < B \leq \infty$

THE GEOMETRY OF SYMMETRIC PERFECT FOLDS

For a particular trapezoid, there is only one possible form of perfect fold that can be inscribed, and therefore the three elements of fold style P, ϕ and b are not independent. I derive this dependence below and use the relationships to show that perfect single-hinged folds are a limiting case for the geometry of possible fold styles.

The relationship among the style elements of perfect folds is derived from the diagrams in Fig. 4. For acute folds, the relations in Fig. 4(a) show that the aspect ratio P is related to the radius of closure curvature r_c and the radius of the reference circle r_0 by:

$$P = \frac{A}{M} = \frac{r_c - r_c \cos \phi/2 + (r_0 - r_c) \sin \phi/2 \tan \phi/2}{2r_0 \sin \phi/2}. \tag{5}$$

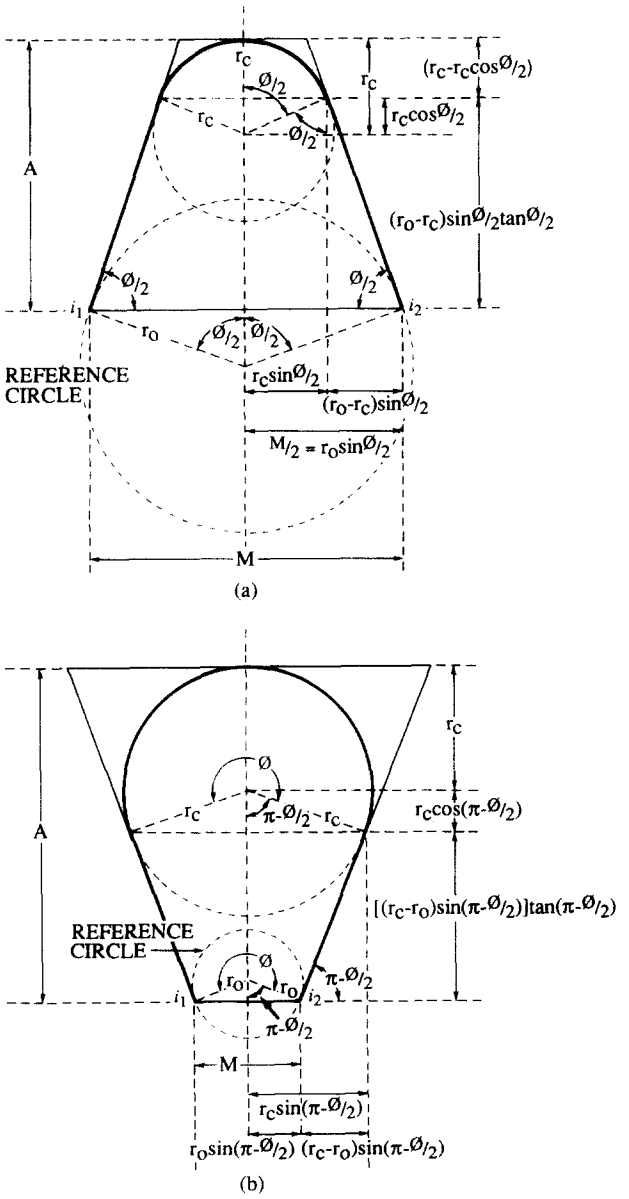

Fig. 4. Geometrical relations from which the dependence of P on B and ϕ for perfect folds is derived. (a) Acute perfect folds. (b) Obtuse perfect folds.

Using equation (2) and standard trigonometric identities, equation (5) can be put in the form

$$P = B \frac{\cos \phi/2 - 1}{\sin \phi} + 0.5 \tan \phi/2. \tag{6}$$

For obtuse folds, the relationship derived from Fig. 4(b) is similar to equation (5) with the angle $\phi/2$ replaced by $(\pi - \phi/2)$ and the signs of the second and third terms in the numerator reversed. This relationship also reduces to equation (6). Thus for both acute and obtuse perfect folds, equation (6) shows that for a constant value of the folding angle ϕ there is a linear relationship between the aspect ratio P and the bluntness ratio B.

The relationship of equation (6) is plotted in the three-dimensional space of log P, ϕ and b in Fig. 5. The form lines depicting the surface are lines of constant ϕ and lines of constant b. The straight lines of constant ϕ in equation (6) become curved with the use of the logarithmic P axis and b instead of B. The contours are drawn only on that part of the surface occupied by perfect folds. Formal extension of the surface beyond these limits is meaningless. The contour for $b = 1$ is a critical boundary for the geometry of perfect folds, and it forms a y-shaped curve that consists of two branches (Fig. 5; see also Fig. 11). One branch is the vertical line at $\phi = 180°$. The other has a low slope for $\phi \leq 180°$ and goes through the point $(P, \phi) = (0.5, 180°)$; as ϕ approaches 360°, the slope tends toward vertical.

The vertical branch of the $b = 1$ contour at $\phi = 180°$ is the plot of all perfect isoclinal folds, and it separates acute from obtuse perfect folds. Because the limbs are parallel, the curvature of the hinge zone is invariant and

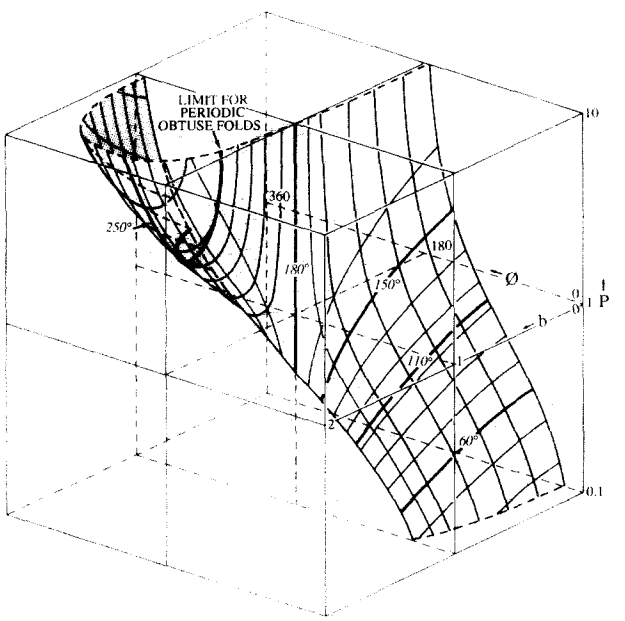

Fig. 5. The three-dimensional surface in fold style space (log P – ϕ – b) that defines the possible geometry of perfect folds. The two sets of contours on the surface are lines of constant b and of constant ϕ. The b contours are at 0, 0.2, 0.4, 0.6, 0.8, 0.9, 1.0, 1.1, 1.2, 1.3, 1.4, 1.5 and 1.7 (cf. Fig. 11). The ϕ contours start at 30° and increase at 15° intervals with the addition of the 110° contour, and the substitution of the 250° for the 255° contour. Heavy ϕ contours are the boundaries of fold tightness categories (Table 2; Figs. 8a and 11).

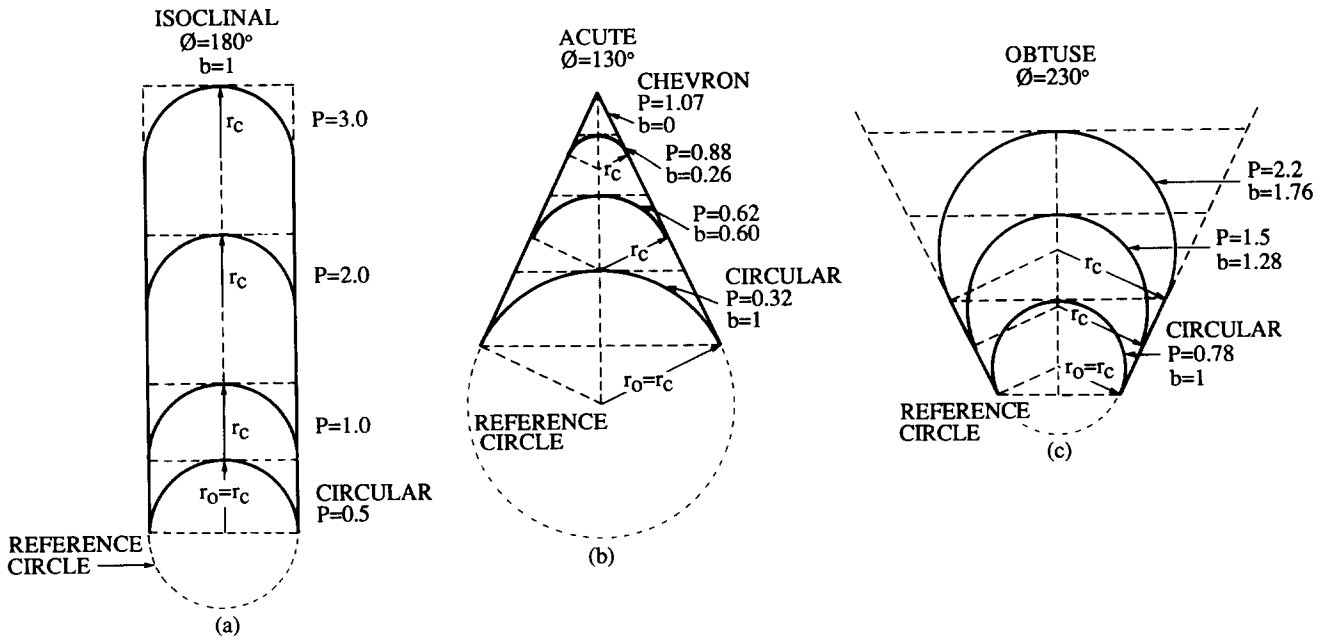

Fig. 6. Perfect circular folds, for which the bluntness $b = 1$, represent a limiting geometry for all perfect folds. (a) For all isoclinal perfect folds, the bluntness must be 1 for all possible aspect ratios. (b) Perfect acute folds at constant ϕ range in bluntness from a minimum of $b = 0$ to a maximum of $b = 1$. (c) Obtuse perfect folds at constant ϕ range in bluntness from a minimum of $b = 1$ for perfect circular folds to a theoretical maximum for individual folds of $b = 2$ at infinite aspect ratio.

thus these folds must always have a bluntness of 1 for all aspect ratios $P \geq 0.5$ ($\log P \geq -0.301$) (Fig. 6a).

The other branch of the $b = 1$ contour is the line of all perfect circular folds, and it represents a maximum possible bluntness for acute perfect folds ($\phi/2 < 90°$) (Fig. 6b) and a minimum possible bluntness for obtuse perfect folds ($\phi/2 > 90°$) (Fig. 6c). This relationship results in the negative slope of lines of constant ϕ for $\phi < 180°$, and the positive slope of these lines for $\phi > 180°$ (Fig. 5). The point where the two branches of the $b = 1$ contour join, i.e. $(P, \phi, b) = (0.5, 180°, 1)$, represents an isoclinal perfect circular fold (Fig. 6a).

Obtuse perfect folds are limited by another geometrical constraint if the folds occur as part of a periodic train of identical folds (Fig. 7). From the relations shown at the top of Fig. 7(a), it is clear that

$$r_c = M \tag{7}$$

and from the relations shown along the median line, we see that equation (4) holds for r_0. Substituting equations (4) and (7) into (2) shows that the bluntness ratio is independent of the aspect ratio

$$B = 2 \sin \phi/2. \tag{8}$$

Thus from equations (8) and (6), the limiting geometry of such folds is completely determined by only a single parameter, which for these equations we can choose to be the folding angle ϕ. The geometry in Fig. 7(b) shows

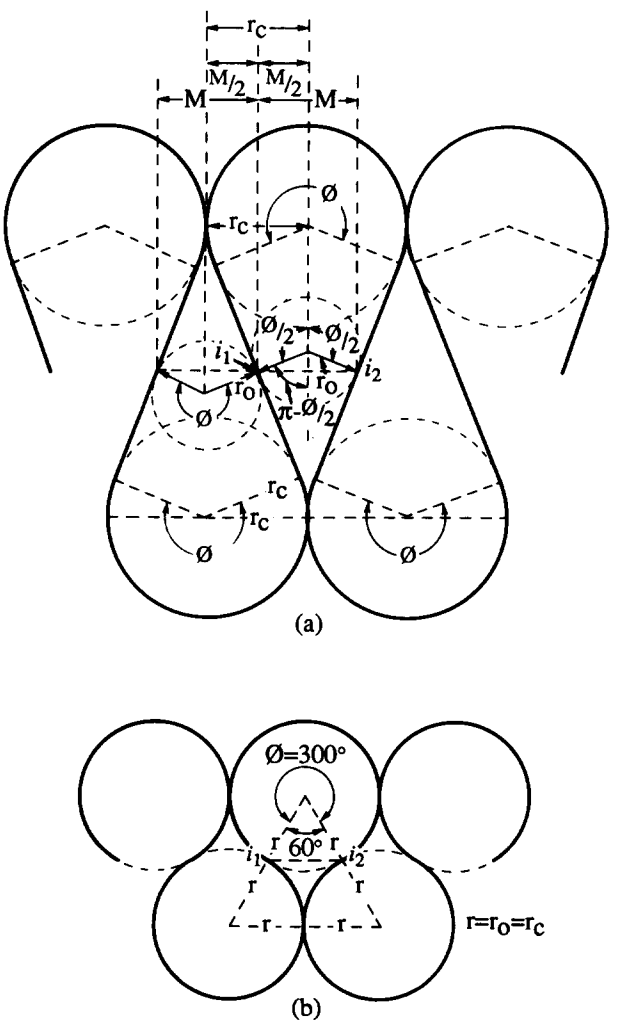

Fig. 7. The limit for the geometry of periodic obtuse perfect folds. (a) Geometrical relations demonstrating that such folds are determined by a single independent parameter. The maximum limit for the bluntness $b = 1.5$ is approached as $\phi/2$ approaches 90°. (b) Geometrical relations showing that the maximum possible folding angle for such folds is $\phi = 300°$ which is for perfect circular periodic folds whose bluntness, $b = 1$, is the minimum possible value for perfect folds.

that for periodic, obtuse, perfect circular folds, the folding angle cannot exceed $\phi = 300°$. Thus in Fig. 5, the line bounding the area of the perfect fold surface on which periodic obtuse folds can plot extends from $\phi = 300°$ at the $b = 1$ line to approach asymptotically the contour for $b = 1.5$ as ϕ decreases towards 180° (cf. equation 8).

THE DESCRIPTION AND CLASSIFICATION OF SYMMETRIC FOLDS

Folds found in nature can hardly be expected to be perfect folds. The values of their style elements, therefore, do not in general plot on the perfect fold surface shown in Fig. 5. That surface, however, represents a boundary between single-hinged and doubled-hinged imperfect folds, as is demonstrated below.

A useful constraint on the possible geometric variation of imperfect symmetric folds of constant folding angle comes from the fact that the integral of the curvature ($d\phi/ds$) along the arc length s of the fold from the inflection point (i) to the closure point (c) must always be half the folding angle

$$\int_i^c \frac{d\phi}{ds}\, ds = \phi/2. \qquad (9)$$

Thus any alteration in geometry that changes the portion of the folding angle subtended by one part of the fold must be associated with a compensating change in the portion of the folding angle subtended by other parts of the fold.

As a means of investigating the geometry and classification of natural folds, it is convenient to examine two-dimensional projections of, and sections through, the three-dimensional space of fold style elements (Fig. 5). The (log P, b) plane and the (log P, ϕ) plane are particularly useful.

Figure 8 shows the (log P, b) plane onto which are projected lines of constant ϕ for different values of ϕ. Figure 8(a) is a projection of all the lines of constant ϕ that mark the boundaries between the various categories of tightness (Table 2). The bluntness of $b = 1$ marks the upper boundary for acute single-hinged folds. The maximum value of b for periodic obtuse perfect folds is always $b \leq 1.5$ (Fig. 7; equations 8 and 3). Figure 8(b) is a section at $\phi = 130°$; Fig. 8(c) is a section at $\phi = 230°$.

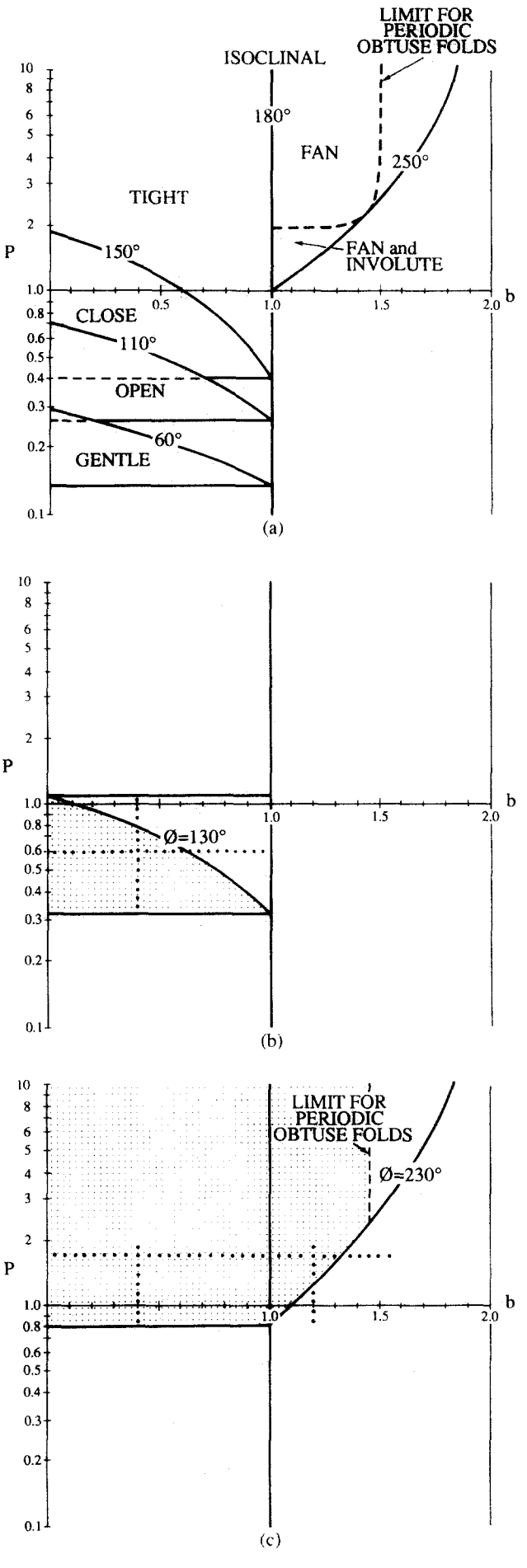

Fig. 8. Projections and sections of the perfect fold surface on the log $P - b$ plane. (a) Projection of the contours of constant ϕ that separate the various categories of fold tightness (Table 2; cf. Fig. 5). Involute folds plot in the same field as some fan folds because along this line of projection the surface defining perfect fold geometry is doubled over (Fig. 5). (b) Section through the perfect fold surface at $\phi = 130°$ illustrating typical relationships for acute folds. Shading shows area in which all acute single-hinged folds must plot. Horizontal solid line indicates the upper boundary for possible acute fold geometry. Fold geometry along the dotted lines is shown in Fig. 9. (c) Section through the perfect fold surface at $\phi = 230°$ illustrating typical relationships for obtuse folds. Shading shows area containing all single-hinged folds. The vertical dashed line is the limit for any periodic single-hinged fold. Fold geometry along the dotted lines is shown in Fig. 10.

These last two sections are representative of the geometric variation possible for acute and obtuse folds, respectively. The shaded areas define the possible range of geometries for single-hinged folds. The possible styles of perfect and imperfect folds that plot on these sections are illustrated in Figs. 9 and 10, respectively, and are described in detail below.

Perfect fold styles at constant ϕ

The sections through fold style space at planes of constant ϕ are particularly useful for understanding the relationship between the styles of perfect folds and associated imperfect folds. Figures 9(a) and 10(a) illustrate how, for a constant folding angle, the aspect ratio and the bluntness are related for perfect fold geometries. For acute perfect folds (Fig. 9a), $b = 1$ represents the maximum possible bluntness, whereas for obtuse perfect folds (Fig. 10a), $b = 1$ represents the minimum possible bluntness. In both cases, the limiting folds are perfect circular folds. The bluntness for acute perfect folds can decrease to $b = 0$, which represents a perfect chevron fold. For obtuse perfect folds, the maximum value of the bluntness is $b < 1.5$ if the folds are part of a periodic fold train (Fig. 7; equation 8). This limit is not absolute, however, as isolated folds can exceed this value (Fig. 10a).

Acute perfect folds are subdivided into categories of bluntness (Table 3), and the fold geometries associated with the category boundaries are shown for perfect folds in Fig 9(a). Obtuse perfect folds have not been formally subdivided and are simply described as blunt folds. They can be distinguished by referring to the particular value of the bluntness (Fig. 10a).

Fold styles at constant ϕ *and* P

Constant values of ϕ and P define a specific shape of circumscribing trapezoid, and the perfect fold associated with that trapezoid defines a maximum possible bluntness for imperfect single-hinged fold styles of both acute and obtuse geometry. Possible style variations are illustrated for acute folds in Fig. 9(b) for $(P, \phi) = (0.6, 130°)$, and for obtuse folds in Fig. 10(b) for $(P, \phi) = (1.7, 230°)$.

Consider the effect of varying b along a line of constant

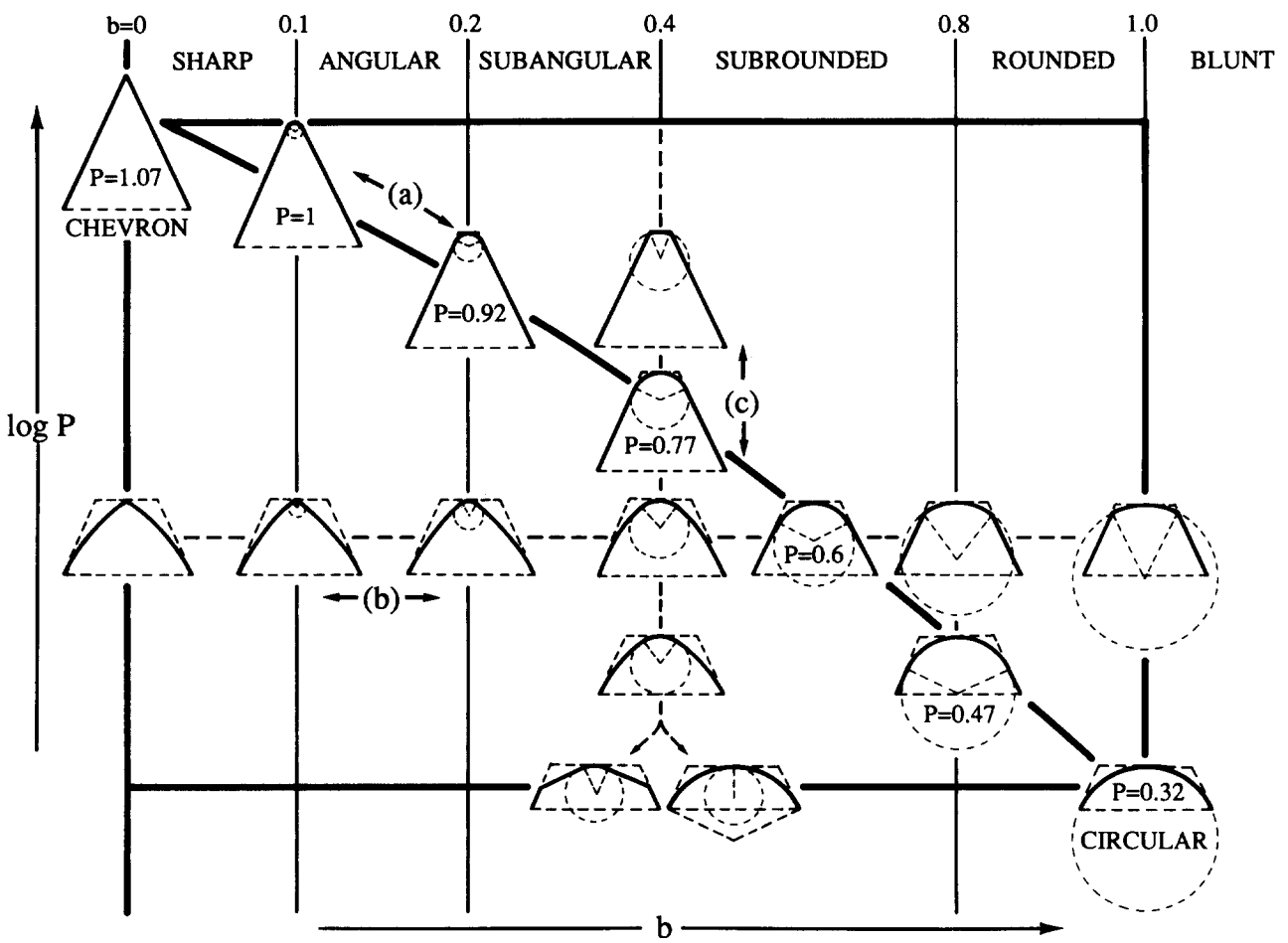

Fig. 9. Fold style variation of acute folds at constant folding angle $\phi = 130°$ showing the bounding geometries for the different classes of bluntness (cf. Fig. 8b). The scales on the log P and b axes are schematic. (a) A series of perfect acute folds of varying bluntness illustrating the dependence of the aspect ratio on the bluntness. (b) A series of acute folds of varying bluntness having a constant aspect ratio and folding angle $(P, \phi) = (0.6, 130°)$. The circumscribing trapezoid is identical for each fold. (c) A series of acute folds of varying aspect ratio having a constant folding angle and bluntness $(\phi, b) = (130°, 0.4)$.

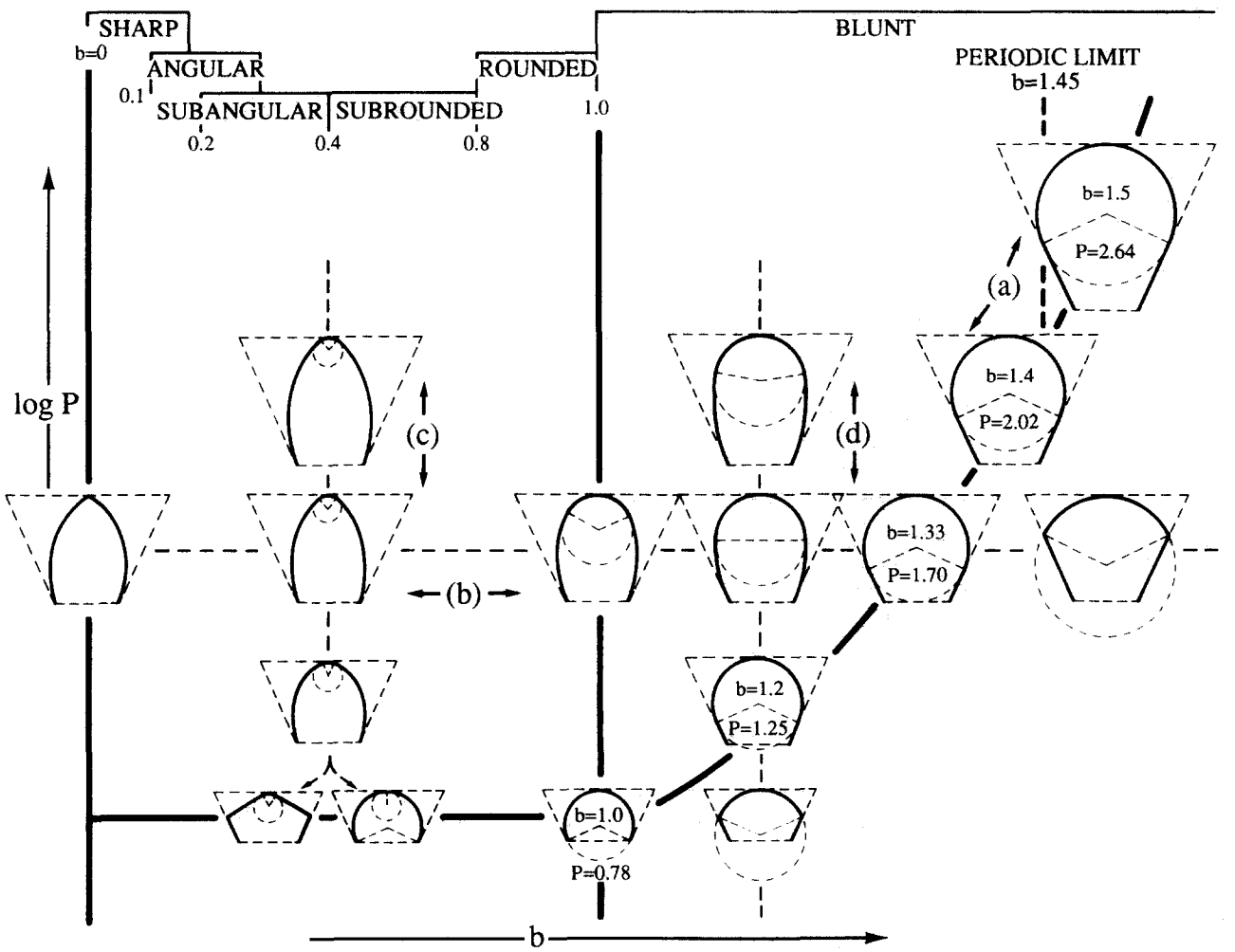

Fig. 10. Fold style variation for obtuse folds at constant folding angle $\phi = 230°$ (cf. Fig. 8c). (a) A series of perfect obtuse folds illustrating the dependence of the aspect ratio on the bluntness at constant ϕ. (b) A series of obtuse folds of varying bluntness having constant aspect ratio and folding angle $(P, \phi) = (1.7, 230°)$. The circumscribing trapezoid is identical for each fold. (c) A series of obtuse folds of varying aspect ratio having constant folding angle and bluntness $(\phi, b) = (230°, 0.4)$. (d) A series of obtuse folds of varying aspect ratio having constant folding angle and bluntness $(\phi, b) = (230°, 1.2)$.

P in a constant ϕ plane, for both acute folds (Figs. 8b and 9b) and obtuse folds (Figs. 8c and 10b). As b increases beyond the value for the associated perfect fold, the angle subtended by the closure zone decreases, and the only way a continuous fold of contant folding angle can be maintained is if a zone of higher curvature, i.e. a hinge zone, is introduced between the inflection point and the closure (equation 9). By symmetry, the resulting fold must be a double-hinged fold. Thus the perfect fold line must be the boundary between single-hinged and double-hinged folds.

Along the same line, as b decreases below the value for the perfect fold, the radius of curvature of the hinge zone decreases (Figs. 9b and 10b). The limbs can remain tangent to the hinge zone only if the limbs become more curved, and the constancy of the folding angle (equation 9) is maintained by decreasing the portion of the folding angle subtended by the hinge zone. For both acute (Fig. 9b) and obtuse (Fig. 10b) folds, the result is a single-hinged imperfect fold geometry. The radius of curvature of the hinge zone can decrease to zero giving $b = 0$.

Fold styles at constant ϕ *and* b

In a plane of constant ϕ, it is impossible to increase the aspect ratio of acute single-hinged folds along a line of constant b beyond the perfect fold geometry. Higher aspect ratios can only be accommodated by double-hinged folds (Fig. 9c, fold geometries for $b = 0.4$). Moreover, the aspect ratio of the perfect chevron fold ($b = 0$) represents an upper bound of P for all possible acute folds of a given folding angle (Figs. 8b and 9c). The aspect ratio can be decreased along a line of constant b if the curvature of the limbs increases and the angle subtended by the hinge zone decreases to satisfy equation (9) (Fig. 9c). This progression can continue until the angle subtended by the hinge zone is zero, at which point the two limbs are tangent at the same point and the fold geometry reverts discontinuously to that of a perfect circular fold, or else a triple-hinged fold must form (Fig. 9c). Thus the aspect ratio of the perfect circular fold is a lower bound of P for all acute imperfect single-hinged folds having the same folding angle.

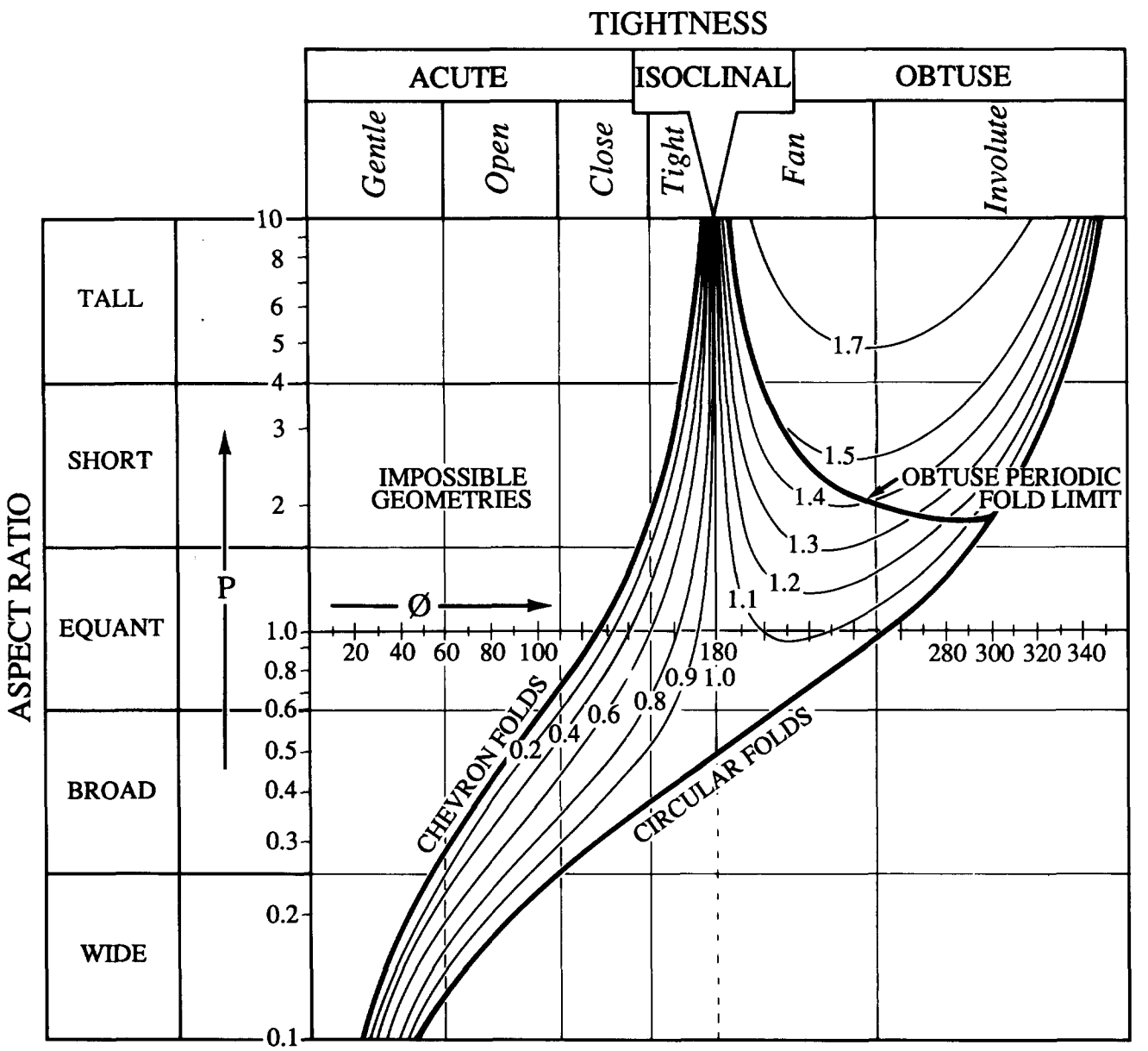

Fig. 11. The trapezoidal system of fold classification is based on a projection of the perfect fold surface in fold style space onto the (log P, ϕ) plane. Contours of constant bluntness b for perfect folds are projected onto the diagram, and these contours represent the maximum possible bluntness for single-hinged imperfect folds. The limit for obtuse periodic perfect folds projects into the upper right quadrant. Classes of tightness are indicated along the top edge, and classes of aspect ratio are indicated along the left side.

For obtuse single-hinged folds in a plane of constant ϕ, there is in principle no upper limit to the aspect ratio along a line of constant b (Fig. 10c & d). As with acute folds, however, the aspect ratio can decrease at constant $b \leq 1$ only to the point that the curvature of the limbs becomes equal to that of the perfect circular fold, at which point either the geometry changes discontinuously to that of the perfect circular fold, or else a triple-hinged fold must form (Fig. 10c, fold geometries along $b = 0.4$). At constant $b \geq 1$, the aspect ratio of obtuse imperfect single-hinged folds can decrease to the value of the associated perfect fold, at which point the fold must become double-hinged (Fig. 10d, fold geometries along $b = 1.2$). Thus the obtuse perfect fold geometry defines a lower limit to the aspect ratio for all obtuse imperfect single-hinged folds.

The maximum value of b for periodic obtuse perfect folds of a given folding angle is also a limit for imperfect folds. Although periodic imperfect folds can have a higher aspect ratio at the same value of b than the associated perfect folds, the bluntness cannot increase beyond the periodic limit without introducing a double-hinged geometry.

Thus, summarizing the relations for acute imperfect single-hinged folds of a given folding angle, we conclude: (1) perfect folds provide an upper limit for values of both aspect ratio P and bluntness b; (2) perfect circular folds define the lower limit of aspect ratio P for all values of bluntness $b \leq 1$; and (3) perfect chevron folds define the upper limit of aspect ratio P for any possible acute fold. Thus acute imperfect single-hinged folds can only plot in a restricted area represented for $\phi = 130°$ by the shaded

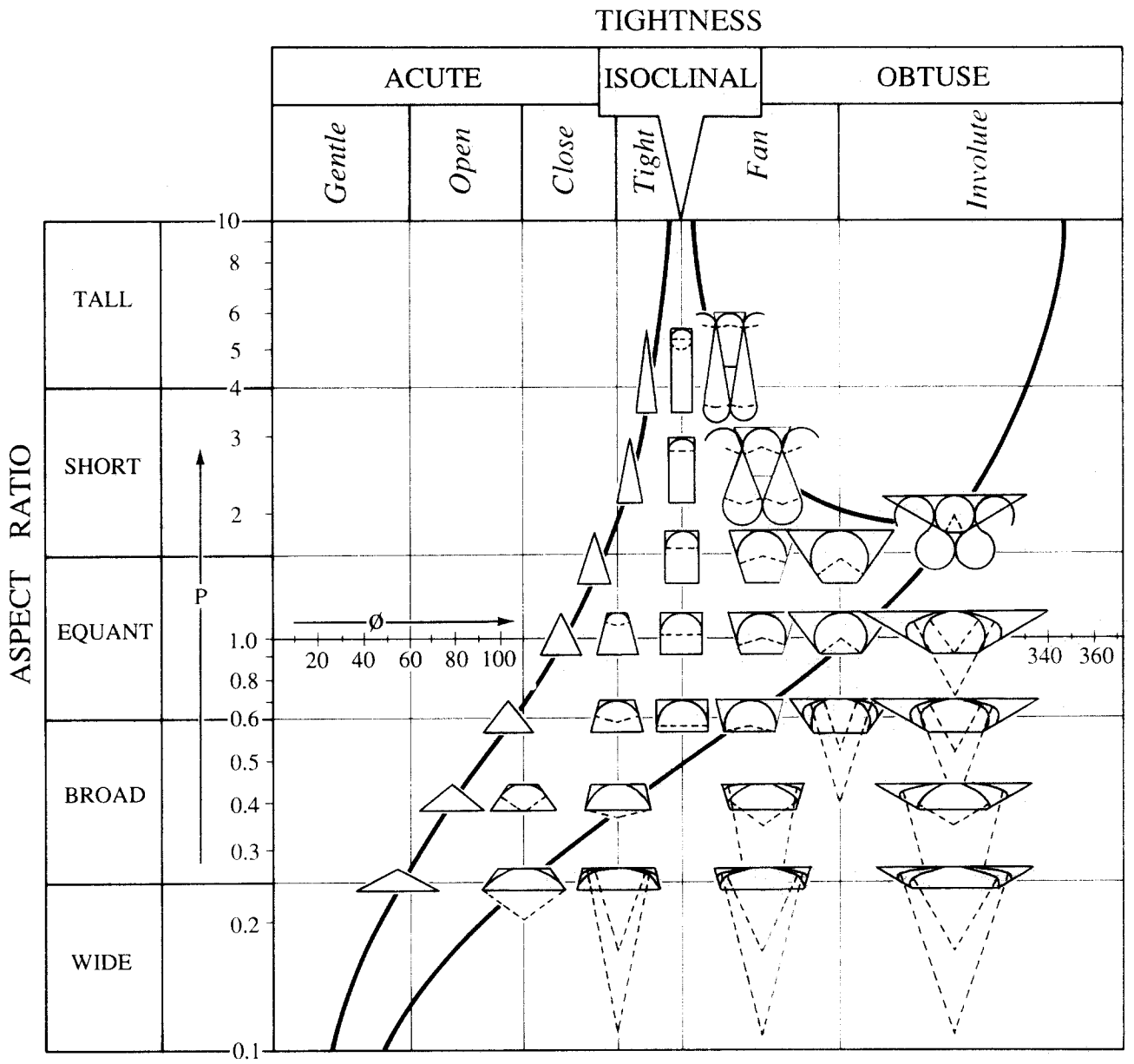

Fig. 12. The trapezoidal system of fold classification, from Fig. 11, showing a sampling of the fold style trapezoids. Perfect folds plot only in the area contoured in Fig. 11 and are shown inscribed in the trapezoids. Outside the area of perfect folds, two possible styles of double-hinged folds are inscribed in each trapezoid. For a given trapezoid, differences in fold style are defined by the bluntness.

area of Fig. 8(b). By extension into the ϕ dimension, such folds are restricted to a volume bounded by the perfect fold surface and by a set of lines extending from the $b = 1$ boundary of that surface parallel to the b axis.

Summarizing the relations for obtuse imperfect single-hinged folds of a given folding angle, we conclude: (1) perfect folds provide a lower limit for values of aspect ratio P for $b \geq 1$ and an upper limit for values of bluntness b; (2) perfect circular folds define the lower limit of aspect ratio P for all values of bluntness $b \leq 1$; (3) the value of bluntness b of the perfect periodic fold defines an upper limit of b for all imperfect periodic folds; and (4) there is no theoretical upper limit to the aspect ratio P for imperfect folds.

The geometry of multiple-hinged folds is not constrained by the relation in equation (6) for perfect folds, so the extension of the surface of acute perfect folds to values of $b > 1$ is meaningless, as is the extension of the surface of perfect obtuse folds to values of $b < 1$. On the projection of fold style space onto the (log P, b) plane, therefore, the bluntness $b = 1$ is the boundary between perfect acute and perfect obtuse folds (Fig. 8a).

Classification of folds on the (log P, ϕ) plane

The most convenient primary classification of folds is provided by the circumscribed trapezoid. A given trapezoid includes a perfect fold and a range of imperfect folds that differ only on the basis of their bluntness. The trapezoids are characterized by the aspect ratio P and folding angle ϕ, and so the (P, ϕ) plane, with a logarithmic P axis, is the most convenient plane to use

for the primary systematic classification of both perfect and imperfect folds.

Figure 11 is a projection of the perfect fold surface of Fig. 5 onto the (log P, ϕ) plane. The boundaries of the different style classes for aspect ratio and tightness are labeled around the perimeter of the diagram, and contours of constant bluntness b for perfect folds are projected onto the plane. Perfect and imperfect single-hinged folds plot only in the area containing these contours, and the contours indicate the maximum possible values of bluntness for the imperfect single-hinged folds (cf. Figs. 9 and 10). The limit for periodic obtuse perfect folds appears in the upper-right quadrant. The area above the perfect chevron fold line ($b = 0$) is an area of impossible fold geometries. The area below the circular fold line ($b = 1$) contains double-hinged folds. For values of bluntness exceeding the contour value, folds in the contoured portion of the diagram are also double-hinged.

Figure 12 shows the outlines of the plot from Fig. 11 with a sampling of the style classes indicated by their circumscribing trapezoids. Within the area where perfect folds plot, each trapezoid is inscribed with the associated perfect fold shape. Outside that area, some of the variation in fold style is suggested by two different inscribed folds.

The examples discussed above indicate that the three style elements P, ϕ and b may be used to classify multiple-hinged folds as well as single-hinged folds. For multiple-hinged folds, however, the bluntness b only describes the curvature of the closure, leaving the curvature of the hinges unspecified. For example, the hinges of double-hinged folds in Figs. 9 and 10 have been drawn as sharp hinges, whereas in Fig. 12 they are shown with some arbitrary bluntness. A more precise characterization requires that the bluntness of the hinges also be specified. The method would be the same as for defining the bluntness of single-hinged folds.

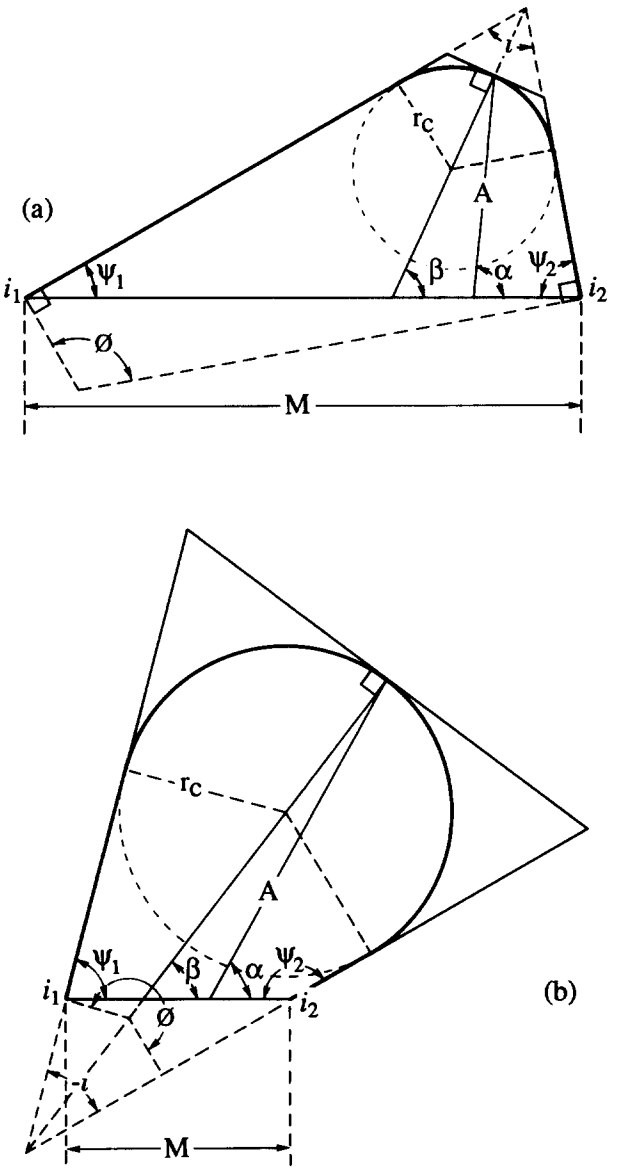

Fig. 13. Elements of fold style for perfect asymmetric folds showing the circumscribing quadrilateral, amplitude A, half-wavelength M, folding and interlimb angles ϕ and ι, and inclination angles β and α for the interlimb angle bisector and the axial surface, respectively. (a) Acute fold. (b) Obtuse fold.

APPLICATION TO ASYMMETRIC FOLDS

The geometry of asymmetric folds

Asymmetric perfect folds of both acute and obtuse geometry, like their symmetric counterparts, are defined to be single-hinged folds composed in profile of perfectly straight limbs which are tangent to a perfectly circular arc that forms the hinge zone (Fig. 13). The asymmetric character of a perfect fold is defined relative to the median line M by two independent angles (Turner & Weiss 1963), the inclination β of the bisector of the interlimb angle ι, and the inclination α of the axial surface (Fig. 13). The first angle is a characteristic of folded surfaces; the second angle is strictly a characteristic of a folded layer or multilayer because at least two nested folded surfaces are required to define the orientation of the axial surface. Nevertheless, isolated folded surfaces are at most rare, and an axial surface can generally be defined for a folded surface. I show below that for the exceptional cases where no axial surface can be defined, the analysis can be done using only the interlimb angle bisector. The two inclination angles α and β are additional style elements that are required to describe perfect asymmetric folds.

A circumscribing quadrilateral is defined for asymmetric folds which has a base M equal to the line segment joining the adjacent inflection points, sides parallel to the fold limbs at the inflection points, and a top tangent to the fold and normal to the interlimb angle bisector (Fig. 13). For perfect folds, the point of tangency is at the hinge and lies on the interlimb angle bisector.

For asymmetric imperfect folds, the closure need not lie on the interlimb angle bisector. To complete the description of asymmetry for imperfect folds, therefore, a third angle τ must be defined (Hudleston 1973) measured from the top of the circumscribing quadrilateral,

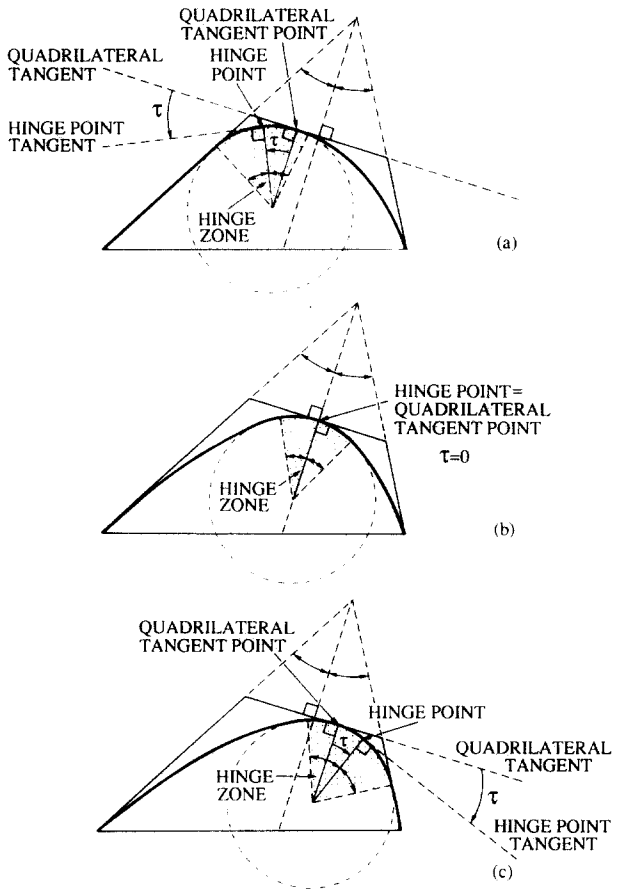

Fig. 14. Definition of the hinge tangent angle τ that is a style element indicating the position of the hinge relative to the interlimb angle bisector. Shaded areas are the hinge zones of each fold. (a) Positive τ. (b) Zero τ. (c) Negative τ.

through the acute angle, to the line tangent to the fold surface at the hinge point (Fig. 14). This angle may be positive (Fig. 14a), zero (Fig. 14b) or negative (Fig. 14c), using the usual definition of counterclockwise angles positive and clockwise angles negative.

The aspect ratio P is again defined to be the ratio A/M (equation 1), where A is the distance from the base M to the top of the circumscribing quadrilateral measured along the axial surface (Fig. 13). The folding angle ϕ is the sum of the two limb angles ψ_1 and ψ_2 measured from the median surface to each limb at the inflection points (Fig. 13). It is also the angle between the normals to the two limbs at the inflection points (Fig. 13). In order to define the bluntness, we must define a reference radius characteristic of the fold. It is not possible to construct a circle tangent to the limbs at both inflection points, so I define r_0 for asymmetric folds by the same equation (equation 4) that defines r_0 for symmetric folds. As α and β increase towards 90°, the fold becomes symmetric, and the definitions for the circumscribing quadrilateral, aspect ratio, folding angle and bluntness become identical to those elements of style defined for symmetric folds.

The equivalent style elements

The classification scheme for symmetric folds (Figs. 11 and 12) can be adapted for use with asymmetric folds by defining for each style of asymmetric fold an equivalent symmetric fold. The transformation from the asymmetric to the equivalent symmetric fold provides definitions of a generalized aspect ratio and a generalized bluntness that apply to both asymmetric and symmetric folds. The relationship among the generalized style characteristics for perfect folds is still represented exactly by equation (6) and by the diagrams of the perfect fold surface in the three dimensional fold style space (Fig. 5). In this section, I derive the generalized forms of the aspect ratio $\hat{P}$, the bluntness ratio $\hat{B}$ and the bluntness $\hat{b}$ (note that circumflexes are used to distinguish the generalized style elements and the quantities that pertain to the equivalent symmetric folds).

An equivalent symmetric fold has the same folding angle as the associated asymmetric fold. To determine the remaining two equivalent style elements (Fig. 15), extend the sides of the circumscribing quadrilateral to their mutual intersection, and construct the bisector of the resulting interlimb angle ι. This line also bisects the folding angle. At the point where this bisector meets the median line M, construct a normal to the bisector. The intersections of that normal with the sides of the circumscribing quadrilateral or their extension define the inflection points $\hat{\imath}_1$ and $\hat{\imath}_2$ on the equivalent trapezoid. The amplitude $\hat{A}$, the half-wavelength $\hat{M}$ and the radius of the reference circle $\hat{r}_0$ for the equivalent trapezoid are all defined as before for symmetric folds. The closure radius of curvature r_c remains unchanged in the transformation from the asymmetric to the equivalent symmetric fold.

Thus the equivalent elements of fold style are defined as before for symmetric folds:

$$\left.\begin{aligned} \hat{P} &= \frac{\hat{A}}{\hat{M}} \\ \hat{B} &= \frac{r_c}{\hat{r}_0} \\ \hat{b} &= \begin{cases} r_c/\hat{r}_0 & \text{for } r_c \le r_0 \\ 2 - \hat{r}_0/r_c & \text{for } r_c \ge \hat{r}_0 \end{cases} \end{aligned}\right\} \qquad (10)$$

and the folding angle ϕ remains unchanged.

Looking first at acute perfect asymmetric folds, we find from Fig. 15(a),

$$\hat{A} = A \cos \delta + A \frac{\sin \delta}{\tan \beta}. \qquad (11)$$

Using standard trigonometric relations and the identity

$$\delta = \alpha - \beta \qquad (12)$$

equation (11) can be written

$$\hat{A} = A \frac{\sin \alpha}{\sin \beta}. \qquad (13)$$

If an axial surface cannot be identified for a fold, measurement of the amplitude along the folding angle besector provides $\hat{A}$ directly.

In the asymmetric fold, the half wavelength M is divided by the bisector of the interlimb angle into two

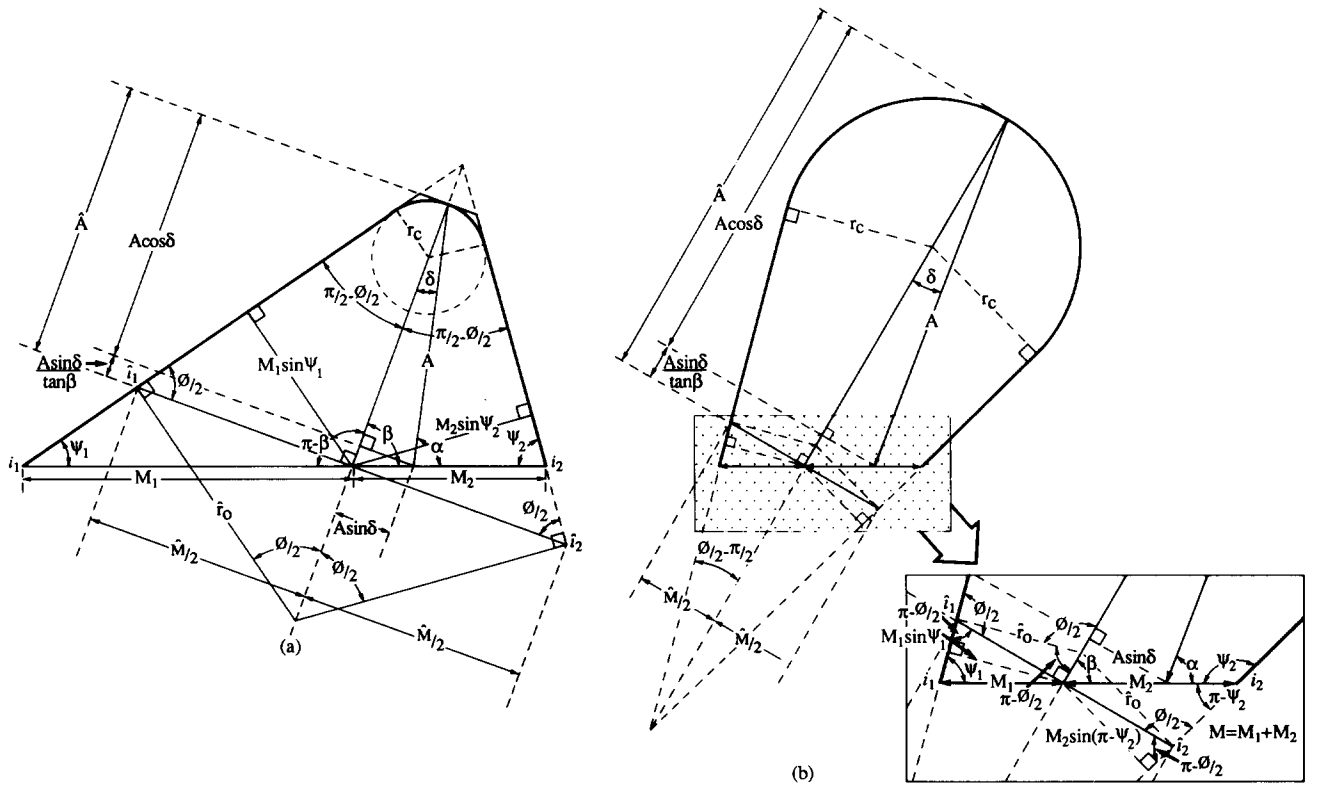

Fig. 15. Geometry for defining the equivalent symmetric fold for a given asymmetric fold. (a) Acute fold. (b) Obtuse fold.

unequal parts M_1 and M_2. Each part is related to the equivalent half wavelength $\hat{M}$ by the relations (Fig. 15a)

$$\left.\begin{aligned}\frac{\hat{M}}{2} &= \frac{M_1 \sin \psi_1}{\sin \phi/2} \\ \frac{\hat{M}}{2} &= \frac{M_2 \sin \psi_2}{\sin \phi/2}\end{aligned}\right\}. \tag{14}$$

Solving these equations for M_1 and M_2, respectively, and using standard trigonometric identities plus the following relations

$$M = M_1 + M_2 \tag{15}$$

$$\left.\begin{aligned}\psi_1 &= \phi/2 + \beta - \pi/2 \\ \psi_2 &= \phi/2 - \beta + \pi/2\end{aligned}\right\} \tag{16}$$

we find

$$\hat{M} = \frac{M}{\sin \beta} \frac{(\sin^2 \beta - \cos^2 \phi/2)}{\sin^2 \phi/2}. \tag{17}$$

The equivalent reference radius of curvature $\hat{r}_0$ (Fig. 15a) is defined in the same manner as shown in equation (4)

$$\hat{r}_0 = \frac{\hat{M}}{2 \sin \phi/2}. \tag{18}$$

Using equation (17) for $\hat{M}$ and equation (4) for the reference radius r_0 of the asymmetric fold, equation (18) becomes

$$\hat{r}_0 = \frac{r_0}{\sin \beta} \frac{(\sin^2 \beta - \cos^2 \phi/2)}{\sin^2 \phi/2}. \tag{19}$$

For symmetric folds, $\alpha = \beta = 90°$ and the equivalent parameters $\hat{A}$, $\hat{M}$ and $\hat{r}_0$ defined in equations (13), (17) and (19) all reduce to the quantities already defined for symmetric folds.

Finally using equations (13), (17) and (19) in equation (10) gives the definition of the generalized aspect ratio $\hat{P}$ and generalized bluntness ratio $\hat{B}$

$$\hat{P} = P \sin \alpha \frac{\sin^2 \phi/2}{(\sin^2 \beta - \cos^2 \phi/2)} \tag{20}$$

$$\hat{B} = B \sin \beta \frac{\sin^2 \phi/2}{(\sin^2 \beta - \cos^2 \phi/2)}. \tag{21}$$

The generalized bluntness $\hat{b}$ is related to $\hat{B}$ by the second and third equations in equation (10). In equations (20) and (21), when a fold is symmetric, α and β both become 90°. Thus the sines of those angles are 1, and in that case the fractions in the equations also become 1, showing that the generalized definitions of aspect ratio and bluntness ratio reduce to the previous definitions for symmetric folds.

For asymmetric obtuse folds (Fig. 15b), all the equations for acute folds remain unchanged, so the final transformation equations (20) and (21) are identical.

Thus using the generalized definitions for aspect ratio $\hat{P}$ and bluntness $\hat{b}$ along with the folding angle ϕ, all folds including symmetric and asymmetric, acute and obtuse, single-hinged and double-hinged, may be classified by the system shown in Figs. 11, 12 and 8(a). For any particular point in fold style space, then, the symmetric and asymmetric folds are distinguished from one another by the values of the two inclination angles β and α for the

interlimb angle bisector and the axial surface, respectively, and the hinge tangent angle τ. Asymmetric folds thus require twice the number of parameters to define their geometry as symmetric folds, and because of this additional complexity less attention is generally given to their geometry.

COMPARISON WITH HUDLESTON'S CLASSIFICATION

Both Stabler (1968) and Hudleston (1973) have proposed that fold forms be described on the basis of the first two odd coefficients of a Fourier sine series fit to various fold forms. Plotting the two Fourier coefficients on orthogonal axes gives a systematic way of organizing the various possible fold styles. Because the determination of Fourier series coefficients is an impractical technique for rapid fold classification, both authors presented fold form charts based on such a plot, and Hudleston proposed a classification system using six 'shape' classes (A–F) and five 'amplitude' classes (1–5). Because Hudleston uses analytic functions as the boundaries for several of his shape classes, it is particularly easy to compare his classification with the one proposed here.

Hudleston's fold style chart is rearranged in Fig. 16 in a format approximately reflecting the relative values of bluntness and aspect ratio of the folds. The six shape classes A–F, within a given amplitude class, correspond in the present analysis to progressively decreasing bluntness (note that in Fig. 16, bluntness increases to the left to facilitate comparison with Fig. 17). The five amplitude classes 1–5 correspond to progressively increasing aspect ratio, and Hudleston's five classes are comparable, but not identical, to the five aspect ratio classes proposed here (cf. Table 1 with aspect ratios listed in Fig. 16). Shape classes A, B and C are inherently isoclinal; for the other three shape classes, the folding angle decreases both downward and to the right toward a minimum in the lower right of Fig. 16.

Hudleston's shape classes A, C, D and F as well as one class intermediate between D and E are analytic functions that are easy to plot in the fold style space of Fig. 5. Shape A folds are box folds, shape C are semi-ellipses, shape D are parabolas, roughly midway between the shapes D and E are sinusoidal folds, and shape F are chevron folds. The equations for the analytic functions, based on a wavelength of 2π, are given by Hudleston as

$$\text{(A) box} \qquad y = k \qquad k > 0,\ 0 \le x \le \pi/2 \tag{22}$$

$$\text{(C) semi-ellipse} \qquad y = +[ax^2 - a\pi x]^{0.5} \qquad a < 0,\ 0 \le x \le \pi \tag{23}$$

$$\text{(D) parabola} \qquad y = ax^2 - a\pi x \qquad a < 0,\ 0 \le x \le \pi \tag{24}$$

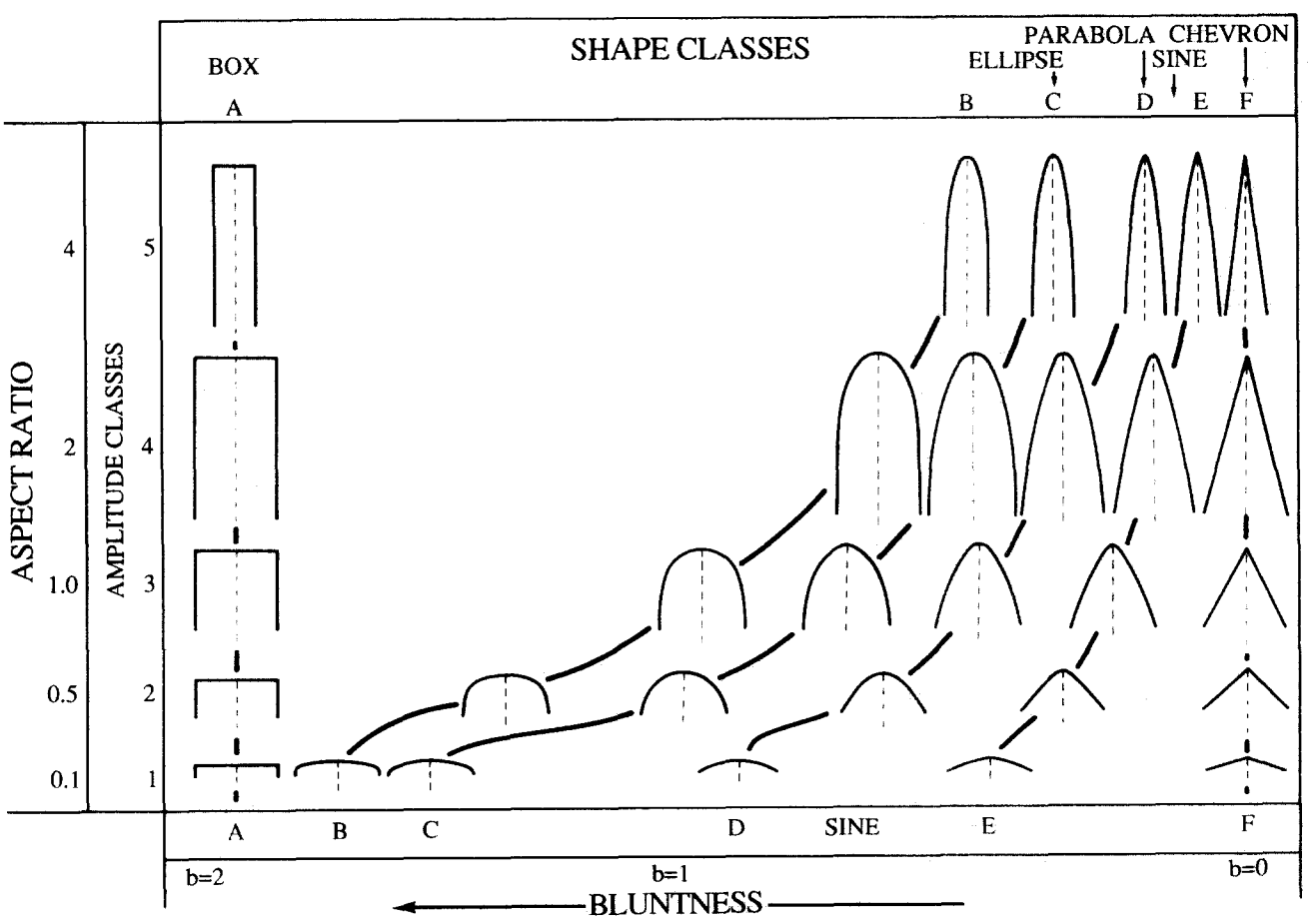

Figure 16. Fold styles in Hudleston's fold classification based on his six 'shape' classes (A–F) and five 'amplitude' classes (1–5). The fold styles are arranged relative to one another according to their aspect ratio and their approximate bluntness. Bluntness increases from right to left. The folding angle is 180° (isoclinal) for shapes A, B and C, whereas for shapes D, E and F it decreases downward and to the right.

sine wave $y = k \sin x \qquad k > 0$ (25)

(F) chevron $y = kx \quad k > 0,\ 0 \leq x \leq \pi/2.$ (26)

The aspect ratio is determined from

$$P = \frac{A}{M} = \frac{y_{max}}{\pi} = \frac{y|_{x=\pi/2}}{\pi}. \tag{27}$$

The folding angle is calculated from

$$\phi/2 = \tan^{-1}(y') \qquad \text{at } x = 0, \tag{28}$$

where y' is the first derivative of y with respect to x. For the radii of curvature required to determine the bluntness, r_0 is determined from equation (4) with $M = \pi$, and r_c is determined from the equation for the radius of curvature of a line, which is presented in standard texts on analytic geometry

$$r_c = \frac{[1 + (y')^2]^{3/2}}{|y''|} \qquad \text{at } x = \pi/2, \tag{29}$$

where y'' is the second derivative of y with respect to x.

The equations defining the fold style parameters determined from equations (22)–(29) are presented in Table 4. The lines in fold style space for shape classes A, C, D, sinusoidal and F are plotted in Fig. 17, and the boundaries for the different 'amplitude' classes are also labeled on the diagram. Shape F is the class of perfect chevron folds which therefore plot along the $b = 0$ line of the perfect fold surface. The sinusoidal and parabolic shapes plot entirely within the acute imperfect single-hinged fold volume. The semi-elliptical folds are isoclinal and therefore are confined to the plane of constant folding angle $\phi = 180°$. Their plot crosses the perfect fold surface from the volume of imperfect single-hinged folds into the volume of double-hinged folds at the intersection with the line of perfect circular folds ($b = 1$). Visual inspection of shape B folds indicates they would plot on the isoclinal fold surface ($\phi = 180°$) at a slightly higher aspect ratio for a given bluntness than the semi-elliptical folds. Shape A box folds also plot on the isoclinal fold surface at constant maximum bluntness ($b = 2$).

The fold style lines in Fig. 17, if projected onto the (log P, b) plane, show relative relations of the fold styles that justify the arrangement shown in Fig. 16. It is apparent from Fig. 16 that Hudleston's classes D5, E5 and F5 differ very little from one another. C5 is also very similar. This similarity is reflected in the convergence of the fold style lines at the high values of log P in fold style space (Fig. 17). There is a major distinction in folding angle between shapes A, B and C on the one hand, and D, E and F on the other. The first three are confined to the plane of isoclinal folds ($\phi = 180°$), whereas the others vary from low folding angles at low aspect ratios to almost isoclinal shapes at high aspect ratios (Figs. 16 and 17). Finally shape A folds are all double-hinged; shapes B and C vary from double-hinged at low aspect ratios to single-hinged at high aspect ratios; and shapes D, E and F are all single-hinged folds (Figs. 16 and 17). These relationships result in a major jump in style at high aspect ratios between the double-hinged shape A and the other five single-hinged shapes, and a smaller jump at low aspect ratio between the double-hinged shapes A, B and C on the one hand and the single-hinged shapes D, E and F on the other.

Thus the fold styles that can be represented by Hudleston's classification are restricted to a specific surface in fold style space, which is approximated by the shaded surface joining the fold style curves in Fig. 17. For acute single hinged folds, that surface is within the volume for imperfect folds and quite close to the surface for perfect folds. At high aspect ratios, the differences between several of the shape classes are relatively minor; double-hinged folds are only represented by isoclinal geometries; obtuse folds are not included at all; and the

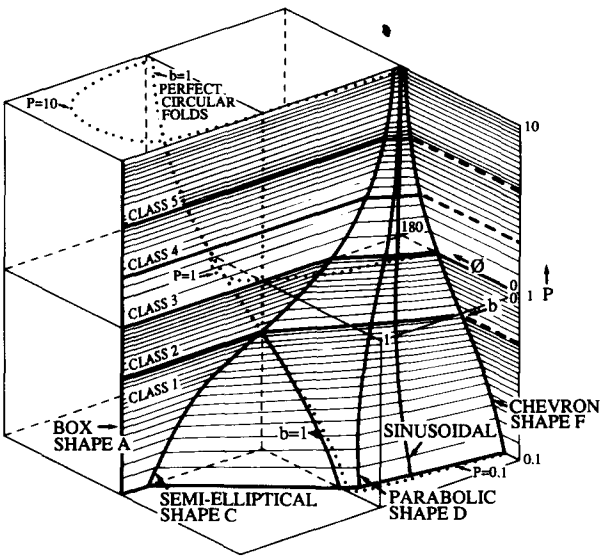

Fig. 17. A plot in three-dimensional fold style space of Hudleston's fold shapes A, C, D, sinusoidal and F, each of which plots as a line. The surface connecting these lines represents approximately Hudleston's two-parameter classification system for folds in single surfaces. Chevron (shape F), sinusoidal, shape E (not plotted) and parabolic (shape D) fold styles all plot within the volume of single-hinged imperfect folds. Shape E folds plot between the sinusoidal and shape F folds. Semi-elliptical (shape C), shape B (not plotted) and box (shape A) folds all plot on the plane of isoclinal folds ($\phi = 180°$). Box folds all plot at $b = 2$; semi-elliptical folds (shape C) plot along a curve that passes from single-hinged imperfect folds to double-hinged folds at $b = 1$. Hudleston's 'amplitude' classes are the labeled lines of constant P. Contours on the perfect fold surface (Fig. 5) for $b = 1$ and for $P = 0.1$, 1 and 10 are shown as dotted lines for comparison. The two surfaces are identical along the line for chevron folds ($b = 0$).

Table 4. Determination of fold style elements for Hudleston's fold classification

Shape class	Aspect ratio (P)	Folding angle (ϕ)	Bluntness ratio (B)
A Box	k/π	180°	∞
B			
C Semi-elliptical	$0.5\sqrt{-a}$	180°	$1/\sqrt{-a}$
D Parabolic	$-a\pi/4$	$2\tan^{-1}(-a\pi)$	$-\sin(\phi/2)/a\pi$
Sinusoidal	k/π	$2\tan^{-1}k$	$2\sin(\phi/2)/k\pi$
E			
F Chevron	$k/2$	$2\tan^{-1}k$	0

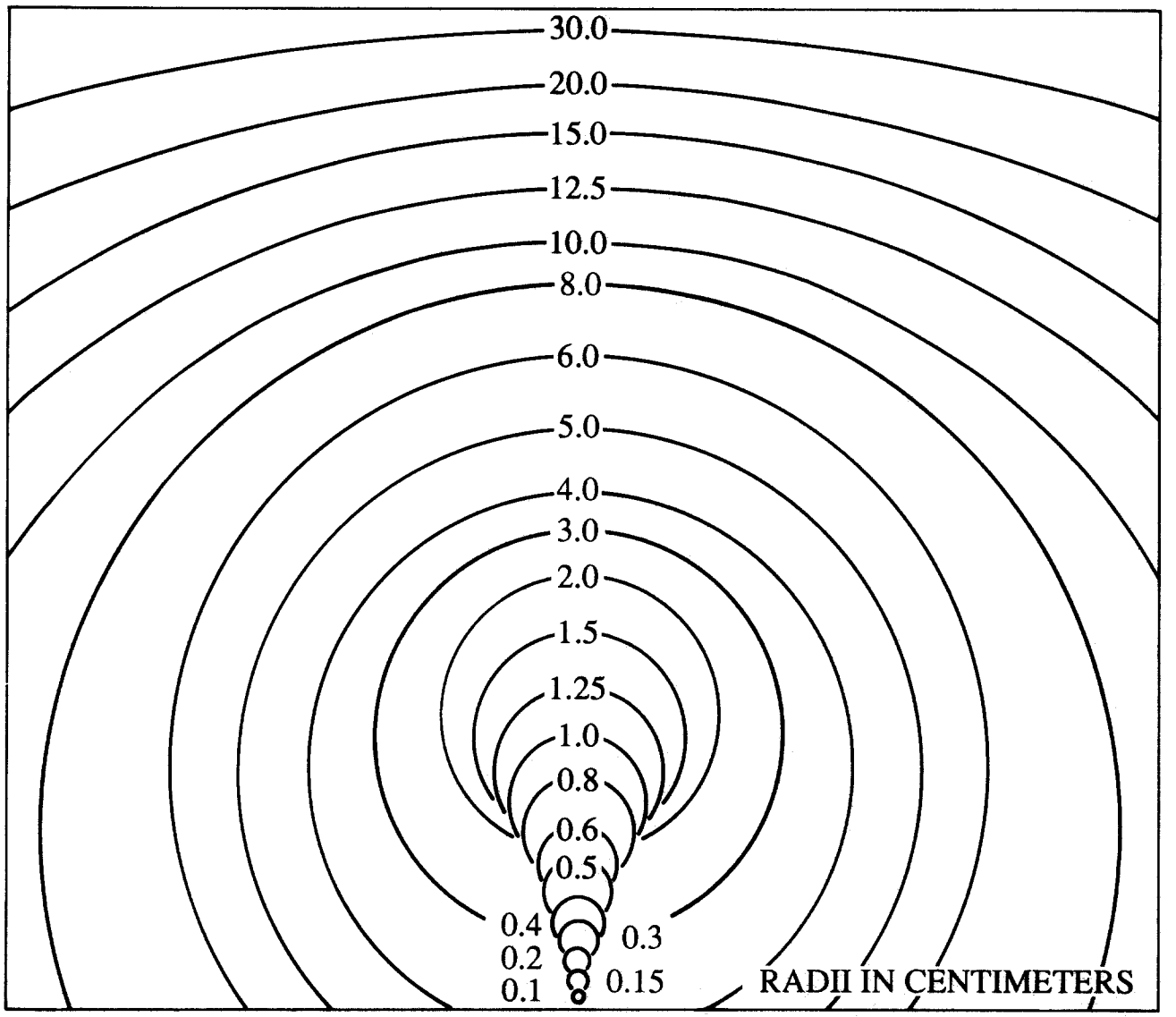

Fig. 18. Template of circular arcs ranging in radius from 0.1 to 30 cm for estimating the closure radius on fold profiles.

folding angle and bluntness are not considered as independent parameters.

CONCLUSIONS

The geometry of folds in single surfaces can be described by three fold style parameters, the aspect ratio P, the folding angle ϕ and the bluntness b. This classification system is a generalization of existing two-parameter classifications. For symmetric folds, the first two parameters are characterics of a trapezoid circumscribing the fold, and that trapezoid is the basis for the primary classification of folds. Within a given trapezoid, different styles of folding are distinguished by the bluntness of the folding, and such styles can range from sharp single-hinged folds, through folds with straight limbs and circular hinge zones, to double-hinged folds.

Perfect folds are an idealized family of folds for which only two of the fold style parameters are independent. They therefore plot on a well-defined surface in the three-dimensional fold style space. Perfect folds are characterized by a single hinge, and perfectly straight limbs tangent to perfectly circular hinge zones. This family of folds defines the limiting values of the fold style parameters for imperfect single-hinged folds, which includes all natural single-hinged folds, and these limits separate single-hinged folds from double-hinged folds.

The classification system is easily applied. Inflection points on folds are relatively easy to locate by eye, so the circumscribing trapezoid is easily identified. The angle between the base and the side of the trapezoid is half the folding angle ϕ, and the ratio of the height A to the base M defines the aspect ratio. These features are also easily measured. The reference radius r_0 is defined in terms of ϕ and M by equation (4). Only the closure radius r_c is somewhat difficult to measure. The simplest method is to use visual inspection to approximate the closure curvature of a fold from a template of circular arcs. One such template with a range of over two orders of magnitude in arc radii is given in Fig. 18. For convenience, the template may be copied onto a transparency and lami-

nated in plastic. For minor folds in the field, the best fitting template curve can be chosen by placing the template directly on the fold profile. For larger folds, the template can be applied to photographs of the fold profile and the radius scaled appropriately.

The same classification scheme can be extended to asymmetric folds, although the description of the fold style for asymmetric perfect folds includes an additional two parameters, the inclination angles β and α for the interlimb angle bisector and the axial surface, respectively. For asymmetric imperfect folds a third parameter, the hinge tangent angle τ is also required.

The proposed classification scheme is more precise and more encompassing than previous schemes. For example Hudleston's widely used classification plots as a specific surface through the proposed three-dimensional fold style space. The volume within which natural single-hinged folds can plot is precisely defined in terms of the three fold style parameters. Other fold styles not included in earlier classifications, such as obtuse folds with a folding angle greater than isoclinal folds, and a wide variety of double-hinged folds, may also be classified with the proposed system.

Acknowledgements—I am grateful to the Geology Department, University of California at Davis, for technical support, and to Janice Fong, who with patience and skill drafted the diagrams.

REFERENCES

Fleuty, M. J. 1964. The description of folds. *Proc. Geol. Ass. Lond.* **75**, 461–492.

Hansen, E. 1971. *Strain Facies*. Springer Verlag, New York.

Hudleston, P. J. 1973. Fold morphology and some geometrical implications of theories of fold development. *Tectonophysics* **16**, 1–46.

Ramsay, J. G. 1967. *Folding and Fracturing of Rocks*. McGraw-Hill, New York.

Stabler, C. L. 1968. Simplified Fourier analysis of fold shapes. *Tectonophysics* **6**, 343–350.

Turner, F, J, & L. E. Weiss 1963. *Structural Analysis of Metamorphic Tectonites*. McGraw-Hill, New York.